Top Catal (2016) 59:219–229
DOI 10.1007/s11244-015-0446-1

ORIGINAL PAPER

Effect of Silylation and Support Porosity of Co/MCM-41 and Co/SiO_2 Catalysts in Fischer–Tropsch Synthesis

Andréia Soares Zola[1] · Lidiane Sabino da Silva[1] · Artur Lemes Moretti[1] · Adriano do Couto Fraga[2] · Eduardo Falabella Sousa-Aguiar[2,3] · Pedro Augusto Arroyo[1]

Published online: 11 August 2015

Abstract The effect of silylation in the performance of cobalt catalysts supported on mesoporous silica MCM-41 and non-porous silica in Fischer–Tropsch synthesis (FTS) at process conditions (240 °C, 10 bar, H_2/CO ratio = 2.15) was evaluated. Catalysts with a concentration of 5 % metallic phase were synthesized by wet impregnation on silylated and non-silylated supports. The catalysts were characterized by nuclear magnetic resonance, X-ray diffraction, N_2-adsorption/desorption, temperature programmed reduction, diffuse reflectance spectroscopy in the ultraviolet visible region and high resolution transmission electron microscope. The characterization analyses showed the silylation treatment cause disorganization and partial blockage in the structure of MCM-41 support. Consequently, it were observed less CO overall conversion and selectivity towards C_{5+} hydrocarbons compared with the FTS catalyst prepared with non-silylated support. Also, according to the results of the catalytic evaluation, CO overall conversion seems to be related to the accessibility of the reactants, whereas log-chain hydrocarbons selectivity relates to the ability to reinsert olefins, in conjunction with metal particle size, which is directly connected with metal-support interaction.

✉ Pedro Augusto Arroyo
arroyo@deq.uem.br

[1] Chemical Engineering Department, State University of Maringá, Av. Colombo 5790, Maringá, PR 87020-900, Brazil

[2] PETROBRAS S.A. CENPES R&D Centre, Cidade Universitária, Av. Horácio Macedo, 950, Cidade Universitária, Rio de Janeiro, RJ 21.941-915, Brazil

[3] Department of Organic Processes, School of Chemistry, UFRJ – CT, Bloco E, Cidade Universitária, Ilha do Fundão, Rio de Janeiro, RJ 21941-909, Brazil

Keywords Fischer–Tropsch · Cobalt species · Mesoporous silica · Silylation · CO hydrogenation · C_{5+} hydrocarbons

1 Introduction

Fischer–Tropsch synthesis (FTS) consists in reacting a synthesis gas with a metal catalyst to form hydrocarbons over a wide size range. The synthesis gas can be obtained from coal, natural gas or biomass. The process is also known as gas to liquid (GTL) technology, because the synthesis derives from gaseous reactants to form products which are preferably in the liquid phase under conditions of ambient temperature and pressure.

Currently, the main driver of the development of GTL technology in Brazil is the use of natural gas reserves. According to the Statistical Yearbook of ANP [1] the total reserves of Brazilian natural gas are 840×10^6 m^3. Of these, 86.1 % were found at the end of 2012, offshore. Rio de Janeiro has the majority (63.3 %), followed by Espírito Santo (12.3 %), São Paulo (11.2 %) and Bahia (3.3 %), the remaining 9.9 % being shared by all other states of the Federation. It is therefore clear that there is a huge market for offshore GTL technology, especially in the south-east of the country.

Moreover, Brazil has excellent prospects in terms of oil and gas in the pre-salt layer, which extends from the coast of Santa Catarina to Espírito Santo, 800 km along the continental coast and 200 km wide [2]. According to Gaspari [3], the best use of this large amount of energy reserves is liquefaction, both to supply the Brazilian market and for export. It should also be remembered that the products obtained by GTL units have significant environmental advantages over traditional products, because they

are produced from a clean fuel [4] and their burning emits virtually no sulphur compounds.

Thus, the current development agenda includes projects to build GTL plants and the improvement of existing and well-established technology, as well as the discovery of new technologies to optimize earlier and later stages of the Fischer–Tropsch reaction. The development of smaller and more modern equipment, energy recovery and development of catalysts have been the main focus of research firms and groups working in this area.

Most catalysts used in this process are based on Ni, Co, Fe and Ru. Among these, cobalt catalysts are the best choice for the FTS when the synthesis gas is mainly obtained from natural gas, because in this case there is a better ratio between cost and CO conversion, enhanced formation of C_{5+} and greater resistance to deactivation [5].

Because of the high cost of cobalt, it is important that the minimum amount of metal is used to maintain the high activity and long effective life of the catalyst. One possible solution would be to produce catalysts on the nanometer scale. However, very small particles of highly dispersed cobalt catalysts can strongly interact with the surface groups of the support during thermal activation treatment. In this conditions the mixed oxides formed are hardly reduced and, consequently, inactive for the Fischer–Tropsch reaction [6].

The literature shows that additional treatments, such as silylation, which provides a hydrophobic surface character, can avoid the formation of agglomerates and thus increase the dispersion of the metal during the impregnation stage [7]. An additional benefit of this type of treatment is that it decreases the interaction between the metallic phase and the support, thus reducing the formation of silicate species [6]. These characteristics can lead to a significant increase in the catalytic activity of the catalysts in the SFT [8].

Another important feature of the support is a porous structure that can control even the particle size of the cobalt supported and hence the metal dispersion in the catalyst [9–12]. Also, the textural parameters of the support can influence the diffusion of reactants and product selectivity [13, 14].

Previous work of our group [15] studied the influence of both the support structure and size of Co particles formed during impregnation in FTS. In general, there is a decrease in catalyst activity when the average cobalt crystallite diameter is increased, and the particle size is proportional to the diameters of the supports used. Furthermore, it was shown that greater accessibility to catalytic sites favours the formation of long-chain hydrocarbons during the reaction, and provides higher levels of overall CO conversion and activity.

Therefore, this study aimed to evaluate the performance of cobalt catalysts supported on mesoporous silica MCM-41 and non-porous silica (Aerosil) in FTS. Samples were prepared by wet impregnation on silylated and non-silylated supports, in order to verify whether this kind of treatment benefits catalysts that have different porous characteristics.

2 Experimental

2.1 Preparation of Catalysts

A mesoporous molecular sieve MCM-41 was synthesized according to the procedure described by Szegedi et al. [16]. We dissolved 3.67 g of CTABr (cetyl trimethylammonium bromide 98 % Vetec) in 66.9 g of deionized water under magnetic stirring and at room temperature. Then, we added 88.6 g of absolute ethanol (99.5 % Nuclear), followed by 24.8 mL of aqueous ammonia (28–30 % Nuclear) and continued stirring for 15 min. Still stirring, we added 7.5 mL of TEOS (tetraethyl orthosilicate 98 %, Sigma-Aldrich) drop by drop. After the addition of TEOS, a gel was formed with the molar composition of 1TEOS:0.3 CTABr:11NH_3:144H_2O:58EtOH. The gel was stirred for 2 h and then left to stand at room temperature for a further 16 h. The precipitate was filtered, washed with deionized water, dried and calcined in an oven at 520 °C for 10 h.

The MCM-41 and non-porous sílica (Aerosil 200) surfaces were silylated in accordance with the procedure described by Martinez and Prieto [7]. The samples were dried at 100 °C overnight and under vacuum at 120 °C for 2 h. Several purges were carried out using N_2 to make the system as dry as possible. Then, a solution of 1,1,1,3,3,3-hexamethyldisilazane (HMDS, Sigma-Aldrich) and toluene was prepared. Using a syringe, we added this solution to the flask containing the solid dried under an inert atmosphere, such that the molar ratio of the mixture was 1SiO_2:0.15HMDS:10toluene. The system was stirred in an inert atmosphere at reflux for 2 h at 120 °C. Then, the silylated solid obtained was filtered, washed several times with toluene and dried at 60 °C in an oven overnight.

The cobalt was incorporated in the supports by conventional wet impregnation using cobalt nitrate solution in ethanol in a rotary evaporator to obtain catalysts with metal loading of 5 % (m/m). The samples were calcined at 300 °C for 4 h. The samples obtained were named of Co/MCM-41, Co/SiO_2, Co/MCM-41(sil) and Co/SiO_2(sil), respectively.

2.2 Characterization of Catalysts

The effect of silylation of the supports was assessed by ^{29}Si solid nuclear magnetic resonance, with a cross-polarization magic angle spinning (CP/MAS) NMR on a Varian

Mercury Plus BB spectrometer. Data were analysed with the aid of the MestReNova 5.3.2 computational package.

The organization of the porous structure was evaluated by X-ray diffraction (XRD) on a Shimadzu XRD-7000 Maxima with a speed of 0.5°/min, 40 kV and 30 mA. To calculate the average diameter of the cobalt crystallites, Scherrer's equation was used.

Analyses of N_2-adsorption/desorption were performed on New 1200 Series equipment from Quantachrome. The samples were activated at 300 °C under vacuum for 3 h, and measured in liquid N_2 (−196 °C).

Analyses of temperature programmed reduction (TPR) were performed in a U-tube type quartz reactor. The samples were previously dried for 90 min at 150 °C and cooled to room temperature. During the measurements, the reducing mixture containing 1.75 % H_2 in argon was passed through the bed of the sample, at the same flow rate of 30 mL/min. The reactor was heated from room temperature to 1000 °C, with a heating rate of 10 °C/min.

The cobalt content effectively incorporated in the samples was determined by atomic absorption spectrometry on Varian 50B equipment.

Diffuse reflectance UV–Visible (DRS/UV–Vis) spectra were obtained using a UV–Vis spectrometer Varian Cary 5G, equipped with a polytetrafluoroethylene (PTFE) sample holder and a quartz window. The diffuse reflectance spectra collected ranged from 200 to 800 nm at room temperature.

High resolution transmission electron microscopy (HRTEM) was carried out using a JEM 3010 URP microscope, at the Electron Microscopy Laboratory of the Brazilian Nanotechnology National Laboratory (LNNano), operating at 300 kV, with an LaB6 thermionic electron gun, and point-to-point resolution of 0.17 nm. HRTEM images were acquired using a charge-couple device (CCD) Gatan 194SC multiscan digital camera, with 1024 × 1024 pixels, attached to the DigitalMicrographTM software™ (Gatan Inc.).

2.3 Catalytic Performance During FTS

The catalytic experiments were performed in a FTS unit with 16 reactors in parallel. First, the catalysts were dried at 120 °C for 3 h. Then, the samples were activated in an atmosphere of pure hydrogen at 400 °C for 10 h. Furnace temperature was slowly reduced to 180 °C. The reaction conditions used for evaluation of the catalysts were based on the conditions described in the literature [15, 17, 18]. Thus, the adopted values were: temperature between 230 and 240 °C; pressure of 10 bar; H_2/CO ratio of 2.15; average reaction time of 170 h and gas hourly space velocity (GHSV) of 1570 h^{-1} which corresponds to a weight hourly space velocity (WHSV) of 9.35 h^{-1}. The reaction products were analysed by gas chromatography. For calculations of conversions and selectivities, the experimental values obtained from the operating condition of the unit and the analyses of reaction products were used. All graphs were plotted using the Origin 8.5 software.

3 Results and discussion

3.1 Nuclear Magnetic Resonance (NMR)

The efficiency of the support silylation was investigated by ^{29}Si nuclear magnetic resonance (NMR), as shown in Fig. 1.

Figure 1 shows the presence in all samples of an intense peak at around −108 ppm which results from the contribution of individual bands at −108, −100 and −90 ppm, assigned to Q^4Si [Si–(O–Si)$_4$], Q^3Si or single hydroxyl groups [OH–Si–(O–Si)$_3$], and Q^2Si or geminal hydroxyl groups [OH_2–Si–(Si–O)$_2$], respectively [7]. For the silylated samples, there was an increase in the peak corresponding to −108 ppm and a decrease in the other two of −100 and −90 ppm, indicating a probable redistribution of silicic sites owed to reactions of the surface SiOH groups with HMDS. The silylated samples also showed an additional peak of 14 ppm, corresponding to silicon atoms bonded to three methyl groups ($Si(CH_3)_3$) [7].

The results confirm the retention of organosilane on the silica surface by the method proposed by Martínez and Prieto [6]. Thus, the surface of the silylated samples was covered with hydrophobic groups, which can theoretically lead to a decrease in the occurrence of silicates in samples after impregnation of the metal.

3.2 X-ray Diffraction (XRD)

The XRD patterns obtained for the samples are shown in Fig. 2. As can be seen in Fig. 2a, the MCM-41 samples exhibited a more intense peak at about $2\theta = 2.3°$, assigned to the reflection plane (100) of the hexagonal structure of mesopores [19, 20]. Less intense and broader peaks, forming 'shoulders' between $2\theta = 4.0°$–$5.5°$, refer to the planes (110) and (200), showing the ordering of the structure. The samples containing cobalt retained these characteristics, whereas the MCM-41(sil) sample showed a decrease in the intensity of the peak at 2.3° 2θ, indicating that the silylation procedure caused a slight decrease in the ordering of the structure.

In Fig. 2b one can observe the diffraction patterns obtained for samples containing cobalt in the range of $5° \leq 2\theta \leq 60°$. Peaks were identified by comparison with JCPDS files, with the aid of the X'Pert HighScore 2.1b (PANalytical BV) computational package. For the samples

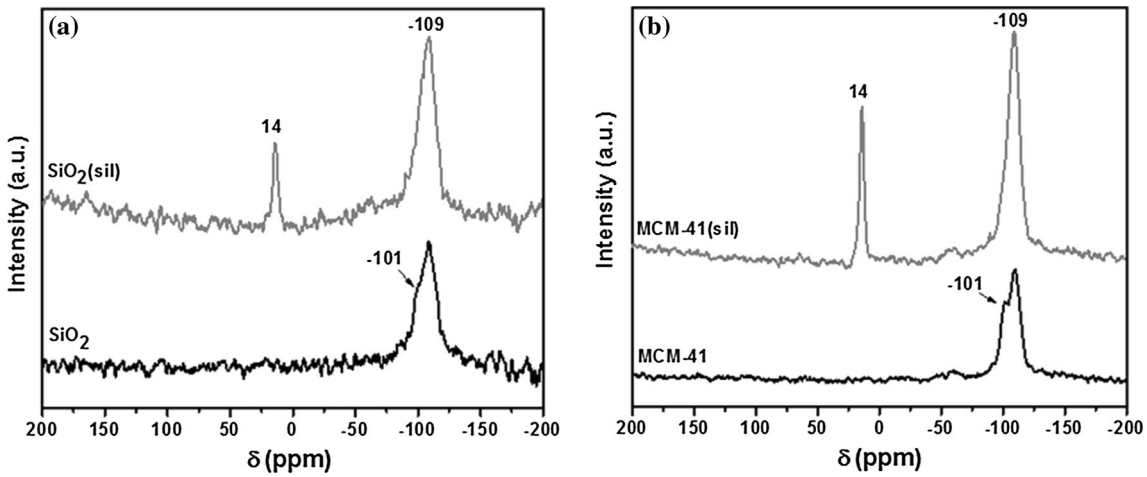

Fig. 1 ^{29}Si NMR spectra for the SiO_2 (**a**) and MCM-41(**b**) silylated and non-silylated supports

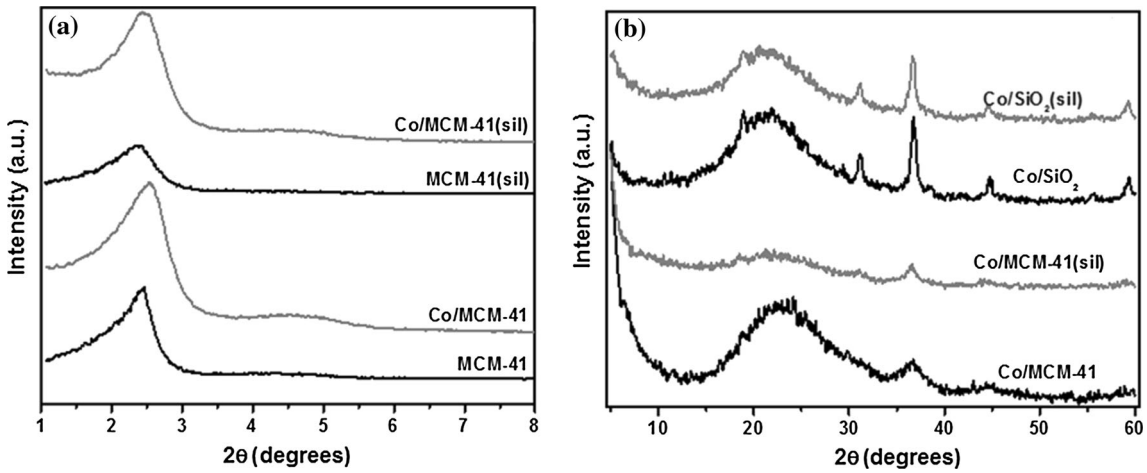

Fig. 2 XRD patterns of supports and samples prepared in the **a** $1° \leq 2\theta \leq 8°$ range and **b** $5° \leq 2\theta \leq 60°$range

of MCM-41, it can be observed one intense peak related to Co_3O_4 (JCPDS 00-009-0418) at approximately $2\theta = 36.9°$. This peak appeared to be stronger for samples prepared on silica, which showed other peaks at $2\theta = 31.3°$, 44.9° and 59.4°, also relating to Co_3O_4 (JCPDS 00-001-1152). In the samples, we also observed a wide peak at 25°, relating to amorphous silica, which may indicate the presence of silicates (Co_2SiO_4) (JCPDS 00-029-0507). The other peaks relating to the silicates may be overlapping peaks of Co_3O_4, because both have spinel structure and, consequently, very close peaks.

Table 1 Average diameter of Co_3O_4 crystallites of the prepared samples

Sample	dp (nm)
Co/MCM-41	4.03
Co/MCM-41(sil)	7.38
Co/SiO_2	15.8
Co/SiO_2(sil)	16.3

Table 1 shows the average diameters of Co_3O_4 crystallites, calculated by Scherrer's equation according to the peak width of the $2\theta = 36.9°$ cobalt oxide. It can be seen that the samples prepared on MCM-41 have smaller cobalt oxide crystallite diameters, indicating that the molecular sieve with small mesopores might not have allowed growth of the particles during the impregnation.

3.3 Adsorption/Desorption of N_2

The isotherms obtained through analysis of the adsorption/desorption of N_2 can be seen in Fig. 3. Samples prepared in MCM-41 exhibited type IV isotherms characteristic of mesoporous solids, whereas samples prepared in SiO_2 exhibited type II isotherms typical of non-porous materials. Additionally, there was a slight hysteresis type H1 in the sample of MCM-41, indicating that the material has irregular pores of cylindrical and/or polyhedral format with

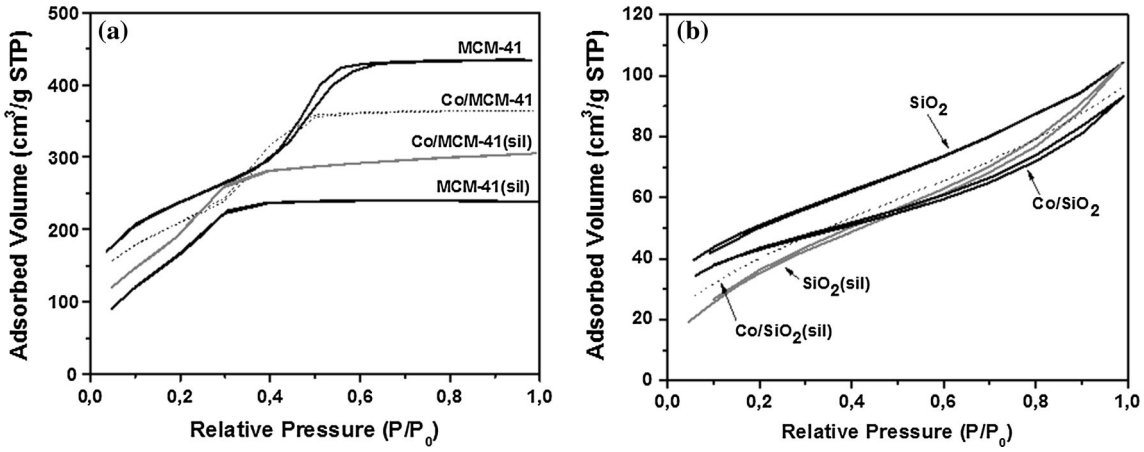

Fig. 3 Adsorption/desorption isotherms of nitrogen **a** MCM-41and **b** SiO_2 samples

Table 2 Textural properties of the prepared samples

Sample	A^a_{surf} (m^2/g)	A^b_{meso} (m^2/g)	A^c_{micro} (m^2/g)	V^d_{porous} (cm^3/g)	D^e_{porous} (nm)
MCM-41	963	309	654	0.757	3.3
MCM-41 (sil)	708	101	607	0.486	2.1
Co/MCM-41	748	202	546	0.547	3.0
Co/MCM-41 (sil)	804	151	653	0.553	2.4
SiO_2	180	65.2	115	0.146	3.6
SiO_2 (sil)	142	84.4	57.6	0.186	4.5
Co/SiO_2	150	58.4	91.6	0.126	3.9
Co/SiO_2 (sil)	152	69.5	82.5	0.157	3.9

[a] Surface area: calculated by BET method

[b] Mesoporous area: calculated by BJH method

[c] Microporous area: calculated by t-plot method

[d] Porous volume: calculated by BJH method

[e] Porous diameter: calculated by BJH method

open ends [21]. In the SiO_2(sil) and Co/SiO_2 samples, there is a hysteresis type H4 characteristic of materials with narrow slit-like pores formed from the particle aggregates [22]. In this case, although we used a non-porous silica as support, the catalyst synthesized from this material had a tendency to form pores because of the presence of aggregates.

Comparing the behaviour of the non-silylated and silylated samples before impregnation of cobalt, we can see that the silylation process caused a decrease in the amount of N_2 adsorbed because of the incorporation of organosilanes which can partially block the pore structure [23].

Table 2 shows the textural parameters of the synthesized samples. The non-silylated samples, after impregnation of the metal, showed smaller values of specific area and pore volume than the silylated support. This suggests the agglomeration of cobalt species partially blocks the pore mouth, and thus hindering the nitrogen access to its interior. However, we saw a different behaviour in the silylated samples: samples containing cobalt showed high amounts of nitrogen adsorbed during analysis (Fig. 3), and higher values of specific surface area (Table 2) compared with the silylated supports. Despite the small difference between the two values, it is possible that during the impregnation the removal of some organosilanes groups occurs, which are larger compared with cobalt, leading to a slight unblock of the pores.

3.4 Temperature Programmed Reduction (TPR)

Figure 4 shows the reduction profiles obtained for the prepared samples. It is possible to observe two peaks at 300 and 360 °C, corresponding to the reduction steps $Co_3O_4 \rightarrow CoO \rightarrow Co$ [24]. Despite the reduction of CoO between 360 and 370 °C, CoO species which interact most strongly with the support may exhibit reduced peaks

between 400 and 500 °C [24]. The peaks observed above this temperature may be attributed to the reduction of cobalt species strongly bounded to the support, such as silicates [25] and/or hydrosilicates [24]. These species are usually called $Co^{\delta+}$.

From the behaviour of the curves it can be seen that the process of silylation did not anticipate the reduction temperature of the species, but caused an increased reduction of $Co^{\delta+}$ species whose peaks appear above 500 °C. This reduction facility may indicate that the cobalt particles are larger on silylated samples, due to less interaction of these species with the support and its consequent agglomeration [6].

Total percentages of reduced cobalt were calculated from the analysis by considering the quantities of cobalt obtained by atomic absorption spectrometry. Moreover, the relative percentage of each cobalt species was calculated from the areas under the reduction peaks taking in account that Co_3O_4 species dominate until 400 °C, CoO species strongly bound to the support appear between 400–500 °C (Co^{n+}) and silicate/hydrosilicates species between 500–1000 °C ($Co^{\delta+}$). The percentage of non-reduced species corresponds to the cobalt species which have strong interaction with the support that prevents their reduction below 1000 °C. The calculated values are shown in Table 3.

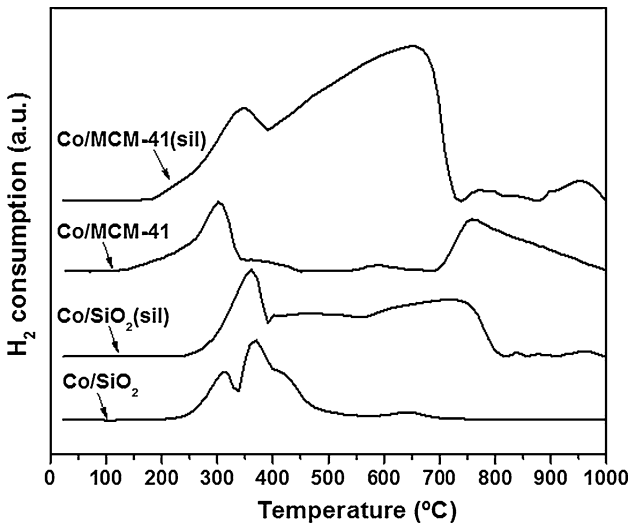

Fig. 4 TPR profiles of prepared samples

First, it can be seen that the silylation process considerably increased the percentage of total reduction (up to 1000° C), especially in MCM-41 samples. However, the percentages of species of Co_3O_4, Co^{n+} and $Co^{\delta+}$ show that despite increasing the overall percentage of reduction, the silylation caused a decrease in the peaks in the reduction of Co_3O_4 and raised areas on the reduction of species of Co^{n+} in MCM-41 and $Co^{\delta+}$ in silica. In other words, the silylation of the surface only contributed to increasing the reducing species that bind more strongly to the support.

3.5 Diffuse Reflectance Spectroscopy in the Ultraviolet Visible Region (DRS)

The DRS analysis was performed on all samples containing cobalt between 200 and 800 nm. According Prieto et al. [26], in this range of wavelength d–d electronic transitions of cobalt ions can be observed. Figure 5 shows the spectra obtained for the prepared samples.

As can be seen in Fig. 5, the samples prepared on MCM-41 showed a peak at approximately 250 nm, suggesting the presence of smaller particles [27, 28] and confirming the results shown by XRD. Near 300 nm, the 'shoulder' mainly observed in the Co/MCM-41 sample corresponds to the nitrate ions remaining after impregnation [29]. In these same samples, a peak can be observed at 400 nm. According to Lim et al. [28], the absorbance between 300 and 400 nm corresponds to the presence of Co^{3+} in a distorted tetrahedral environment or cobalt species on the outer surface of the support. This same peak appears in SiO_2 samples shifted to 430 nm, similarly to Co^{3+} ions in the octahedral ordered manner [30, 31].

Between 600 and 800 nm, a less intense peak can be observed at around 700 nm for all samples. Between 550 and 700 nm, the absorbance can be attributed to the presence of Co^{2+} in a tetrahedral coordinated manner on the support [32]. Slightly above 700 nm, we see a band resulting from the decomposition of cobalt nitrate [29], indicating the oxygen-metal charge transfer for the Co^{3+} feature of the spinel structure of Co_3O_4 [26]. The presence of Co_3O_4 and nitrate ions was expected because the samples were prepared by wet impregnation with cobalt nitrate

Table 3 Total percentage of reduction and contribution of each species of cobalt obtained from TPR analysis

Sample	Metal loading (%m/m)	Percentage of reduction	Species (%)		
			Co_3O_4	Co^{n+}	$Co^{\delta+}$
Co/MCM-41	4.69	21.8	42.9	1.43	55.7
Co/MCM-41(sil)	5.21	100	21.4	18.2	60.4
Co/SiO_2	4.98	57.5	62.2	26.3	11.5
Co/SiO_2(sil)	4.92	65.7	25.8	16.9	57.3

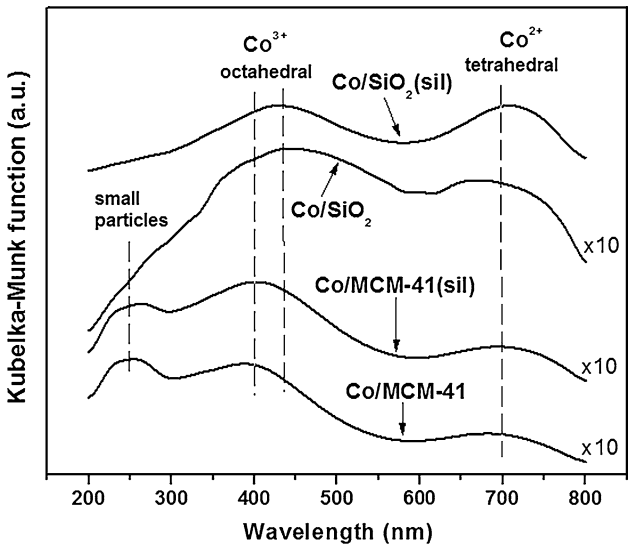

Fig. 5 DRS spectra for prepared samples

under atmospheric air, thus promoting the formation of metal oxide species.

3.6 High Resolution Transmission Electron Microscopy (HRTEM)

HRTEM was performed on the Co/MCM-41 and Co/MCM-41(sil) samples to observe the silylation effects, shapes and sizes of cobalt particles on the support. Figure 6 shows the images in lower magnification (8000 and 50,000 times) of the Co/MCM-41 sample. In this magnification, the images were very similar for both samples.

In Fig. 6a it is clear that the MCM-41 particles are spherical, large and irregular size, mostly around 0.5 µm. At 50,000 times magnification, Fig. 6b, it can be seen that the cylindrical pores of the MCM-41 are concentric and have diameters of about 3.0 nm, agreeing with the results obtained by adsorption/desorption of nitrogen.

Figure 7 shows HRTEM analysis of the Co/MCM-41 sample at higher magnifications. It must be noted that the edges of cobalt particles are uneven, Fig. 7a, and very small (around 2 nm). Widening the image even more, Fig. 7b, reveals some spherical particles in the sample, some with diameters of about 2 nm. Interplanar spacings of 0.016 nm and 0.173 nm were found, equivalent respectively to metallic Co and $CoSiO_3$.

Figure 8 shows HRTEM images of the Co/MCM-41(sil) sample. It can be seen that the shapes of the particles are similar to those at the edges of non-silylated sample, with a size of around 2 nm. The interplanar distance of these particles was 0.150 nm, which is caused by the cobalt oxide (CoO). However, one should take into consideration some caveats. The cobalt particles have extremely small size and inadequate contrast with the support, which make it difficult to visualize clearly the metal species inside the catalyst. However, the little lighter images at the edges enable to visualize the atomic planes of the cobalt species. Therefore, the fact that particle only be CoO is not a significant result, as many other species of cobalt not displayed are located in the centre of the silica particles.

According to the obtained images, the samples showed a mixture of very small particles within the pores (not seen) and edges, including cobalt agglomerates. Therefore, the average particle diameter measured by XRD can vary widely. Through these results, we can conclude that the diameter of the cobalt particles supported on MCM-41 depends strongly on the pore diameter, especially when it comes to samples prepared by wet impregnation, without size control.

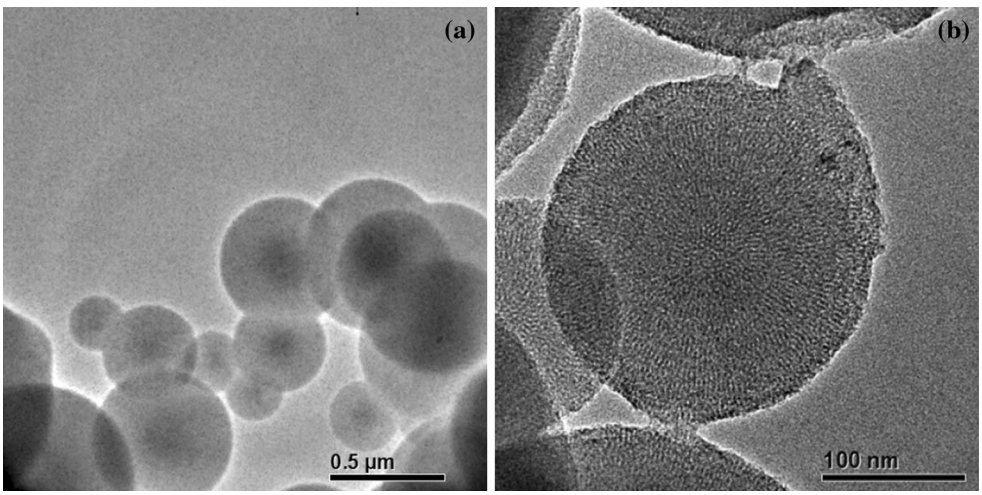

Fig. 6 HRTEM images of the Co/MCM-41 sample: **a** magnified 8000 times and **b** magnified 50,000 times

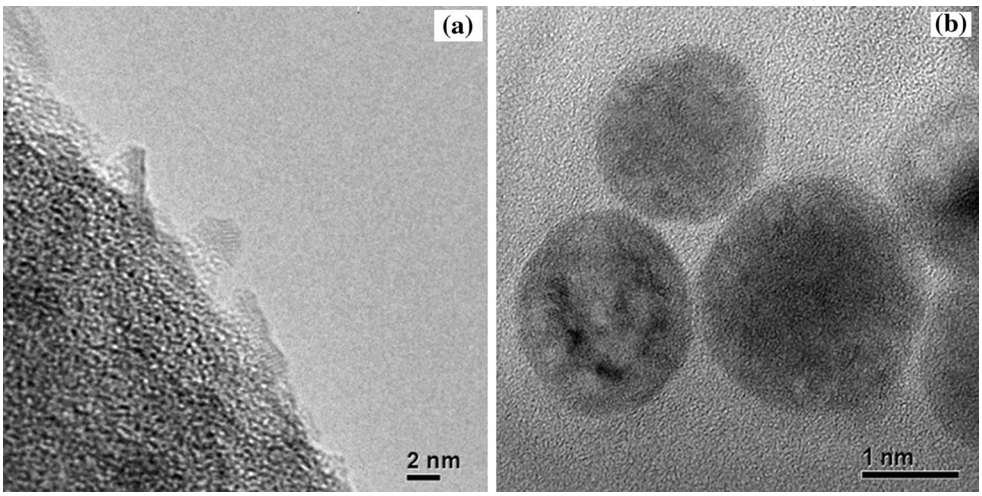

Fig. 7 HRTEM images of the Co/MCM-41 sample: **a** magnified 600,000 times and **b** magnified 1,000,000 times

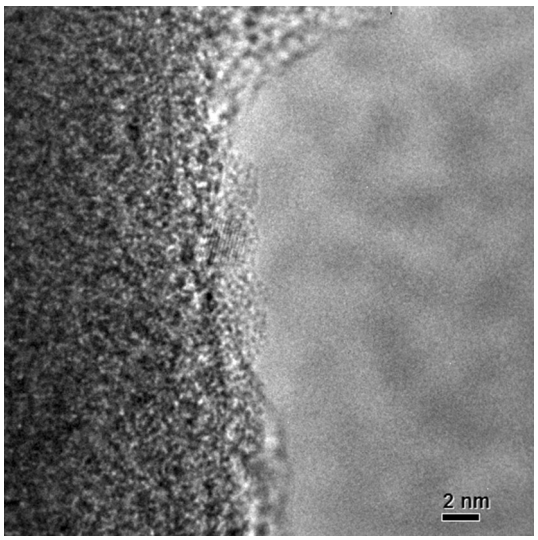

Fig. 8 HRTEM images of the Co/MCM-41 (sil) sample magnified 600,000 times

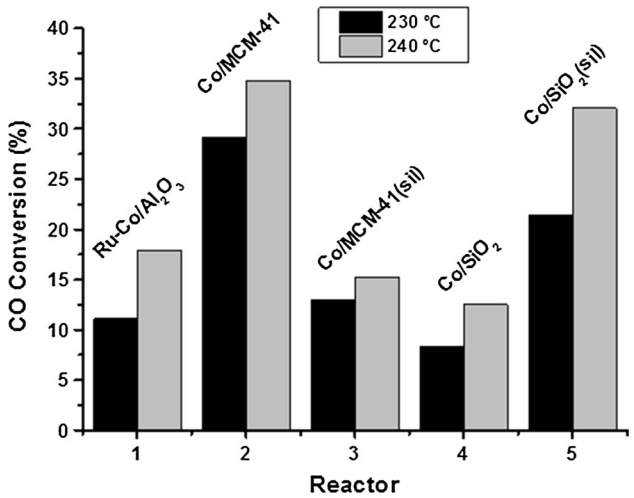

Fig. 9 CO overall conversions as a function of temperature for Fischer–Tropsch reaction

3.7 Catalytic Performance During FTS

The tests were carried out in two steps with a milder temperature (230 °C) to begin with which was then raised to 240 °C. This procedure was adopted because the TPR results observed indicated the need for a little higher temperature than usual to reduce the Co supported.

The values of the CO overall conversion for each sample tested are shown in Fig. 9. Co/MCM-41 (reactor 2) and Co/SiO_2 (sil) (reactor 5) samples had better results for overall conversion and were even very close to the standard catalyst (Ru-Co/Al_2O_3) tested for comparison effect.

The results indicate that the surface silylation contributed positively to the performance of SiO_2 samples, because the silylated sample showed higher values for CO conversion compared with non-silylated, as also verified by Jia et al. [33]. In this case, it can be suggested that the HMDS reacted with the silanol groups of the silica, decreasing the metal-support interaction and providing a gain in the reducibility of cobalt species. However, there is an opposite effect for MCM-41 samples. As observed through analyses of adsorption/desorption of nitrogen and XRD, the silylation of MCM-41 caused a disruption in the structure and porosity partial blockage, which meant the silylated sample presented a worse performance than the sample non-silylated in the FTS because of an decrease in the accessibility of reagents.

Figure 10 shows the FTS product distribution of each sample. These values were calculated only for the testing realized at 230 °C because of a blockage in the detector pipe at 240 °C. The C_{5+} selectivity refers to hydrocarbons

with up to 17 carbons, since this value for larger chains was close to zero.

For the Ru-Co/Al_2O_3 standard sample, the distribution of products is dominated by C_{5+} hydrocarbons. It is clear, then, that the heavy fraction is maximized for this catalyst. Similar product distribution can be observed for the Co/SiO_2 sample (reactor 4). Although this sample did not present the highest value of CO overall conversion, the syngas was mostly converted to C_{5+} hydrocarbons.

The Co/MCM-41 (sil) (reactor 3) and Co/SiO_2(sil) (reactor 5) samples also showed a greater contribution of C_{5+} fraction. Reverse behaviour was observed in which silylation had a positive effect on C_{5+} selectivity for MCM-41 samples, but on overall conversion only for SiO_2 samples. That is, some samples showed high values of overall conversion and at the same time lower selectivity regarding heavier hydrocarbon products.

One explanation for the increased selectivity regarding C_{5+} hydrocarbons of some samples seems to be related to particle size. According to the results, a greater pore diameter leads to the formation of larger metal particles which appear to be more selective regarding long-chain hydrocarbons. According to Tang et al. [34], larger particles favour adsorption of bridged CO, which dissociates more easily than linear CO, leading to the formation of the CH_2 groups necessary for chain growth. This is in accordance with the highest values of the C_{5+} selectivity of the catalysts supported on SiO_2.

The products of FT synthesis follow the Anderson–Schulz–Flory (ASF) distribution because of the polymerization mechanism [35]. According to ASF distribution, ideally, the molar fraction (W_n) of the hydrocarbon product with a carbon number of n is only dependent on the chain-growth probability (α), which is a function of the rates of chain growth and chain termination, by the following equation:

$$W_n/n = (1-\alpha)^2\alpha^{n-1} \quad (1)$$

In other words, the product selectivity is determined by α value between 0 and 1. A smaller α value leads to lighter hydrocarbons, while higher α value results in the formation of heavier hydrocarbons. Therefore, for better understanding of the results, the values of chain growth probability factor

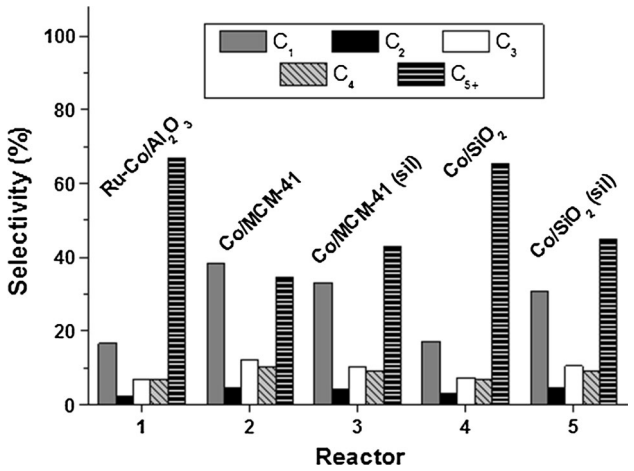

Fig. 10 Selectivities regarding FTS products

Table 4 Chain growth probability (α) of the samples tested

Sample	α
Co/MCM-41	0.72
Co/MCM-41(sil)	0.75
Co/SiO_2	0.83
Co/SiO_2(sil)	0.76
Ru-Co/Al_2O_3	0.84

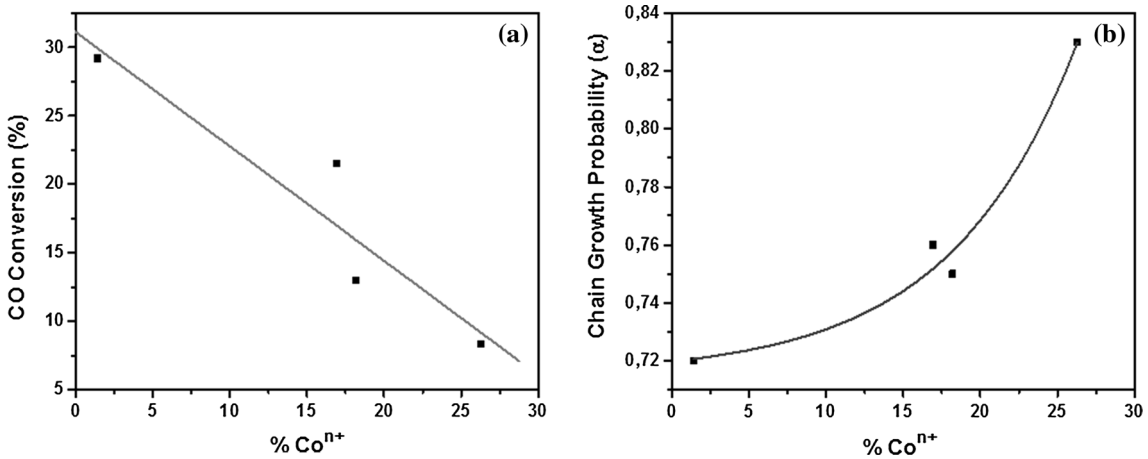

Fig. 11 Correlation between the percentage of Co^{n+} species obtained by TPR and **a** CO overall conversion at 230 °C and **b** chain growth probability factor (α)

(α) of all samples were calculated. The α values obtained are presented in Table 4.

As can be seen in Table 4, the Co/SiO_2 sample shows a value of chain growth probability closer to the value of the standard catalyst. The other samples have α values close to each other, ranging from 0.72 to 0.76.

Figure 11 shows the correlation between the number of Co^{n+} species, and the values obtained for CO overall conversion at 230 °C and the chain growth probability factor (α).

As can be seen, the CO overall conversion decreases linearly when an increasing number of species interact strongly with the support (Co^{n+}). In addition, the chain growth probability factor increases exponentially as higher number of these species are observed. Thus, the amount of Co^{n+} may explains the contrary behaviour of some samples when values of conversion and selectivity are compared. The Co/MCM-41 sample that showed the highest conversion, for example, showed the lowest value of α, so this sample had lower numbers of species with stronger bonds with the support, reducible between 400 and 500 °C.

The results suggest that the performance of FTS catalysts depends on several interconnected factors. The support chosen should allow species to be reduced in the presence of hydrogen, but at the same time there is a certain interaction which ensures the maintenance of the size distribution of cobalt metal particles on the support surface. CO overall conversion seems to be related to the accessibility of the reactants, whereas selectivity relates to the ability to reinsert olefins in conjunction with the metal particle diameter, which is directly connected to the metal-support interaction. Thus, an optimized catalyst would be one that can add these two features. The use of mesoporous molecular sieves appears promising, but because of low thermal stability it would interesting to use a more stable and even larger pore support.

4 Conclusions

In the present work it was shown that Co/MCM-41 and Co/SiO_2(sil) samples gave the best results for CO global conversion in FTS, indicating that silanization harmed the porosity of MCM-41 and may have affected the performance in relation to the non-silylated sample. Besides, for the SiO_2 the HMDS reacted with silanol groups, decreasing the metal-support interaction and improving its performance in relation to the non-silylated sample. Thus, CO overall conversion seems to be related to the accessibility of the reactants to the active site. The long-chain hydrocarbons selectivity observed is related to the reinsertion of olefins in conjunction with the particle diameter, which is directly related to the metal-support interaction. Therefore, the improvement in the reactants accessibility, along with control of particle size and metal-support interaction, which allows better dispersion of the metal particles, is a key feature in obtaining catalysts with high CO conversion and selectivity to long-chain hydrocarbons in FTS.

Acknowledgments The authors are grateful to Coordination for the Improvement of Higher Education Personnel (CAPES/Brazil), National Council of Scientific and Technological Development (CNPq/Brazil) for financial support and The Brazilian Nanotechnology National Laboratory (LNNano) for HRTEM analyses.

References

1. Anuário Estatístico Brasileiro do Petróleo, Gás Natural e Biocombustíveis (2014) BR, Rio de Janeiro, Rio de Janeiro. http://www.anp.gov.br. Accessed 22 Jan 2015
2. Ramos ALD, Marques JJ, Santos V, Freitas LS, Santos RGVM, Souza MMVM (2011) Atual estágio de desenvolvimento da tecnologia GTL e perspectivas para o Brasil. Quim Nova 34:1704–1716
3. Gaspari A (2008) 'Saída liquefeita', Retrospectiva oil and gas. Brasil Energia 335:8–10
4. O Renascimento de uma Tecnologia Madura: O processo Fischer-Tropsch de Conversão de Gás em Combustíveis Líquidos (2002) BR, Rio de Janeiro, Rio de Janeiro. http://www.gee.ie.ufrj.br/publicacoes/pdf/2002_renasc_tec_madura.pdf. Accessed 4 Aug 2012
5. Davis BH (2003) Fischer-Tropsch synthesis: relationship between iron catalyst composition and process variables. Catal Today 84:83–98
6. Martínez A, Prieto G (2007) The key role of the support surface tuning during the preparation of catalysts from reverse micellar—synthesized metal nanoparticles. Catal Commun 8: 1479–1486
7. Martínez A, Prieto G (2007) Breaking the dispersion-reducibility dependence in oxide-supported cobalt nanoparticles. J Catal 245:470–476
8. JungáKim D, ManáKim J (2005) Enhancement in the reducibility of cobalt oxides on a mesoporous silica supported cobalt catalyst. Chem Commun 11:1462–1464
9. Fu T, Lv J, Li Z (2014) Effect of carbon porosity and cobalt particle size on the catalytic performance of carbon supported cobalt Fischer-Tropsch catalysts. Ind Eng Chem Res 53: 1342–1350
10. Tao CL, Li JL, Liew KY (2010) Effect of the pore size of Co/SBA-15 isomorphically substituted with zirconium on its catalytic performance in Fischer-Tropsch synthesis. Sci China Chem 53:2552–2559
11. Khodakov AY, Bechara R, Griboval-Constant A (2003) Fische–Tropsch synthesis over silica supported cobalt catalysts: mesoporous structure versus cobalt surface density. Appl Catal A 254:273–288
12. Khodakov AY, Griboval-Constant A, Bechara R, Zholobenko VL (2002) Pore size effects in Fischer Tropsch synthesis over cobalt-supported mesoporous sílicas. J Catal 206:230–241
13. Lualdi M, Lögdberg S, Carlo G, Järas S, Boutonnet M, Venezia AM, Blekkan ED, Holmen A (2011) Evidence for diffusion-controlled hydrocarbon selectivities in the Fischer–Tropsch synthesis over cobalt supported on ordered mesoporous silica. Top Catal 54:1175–1184
14. Martínez A, Prieto G, Rollan J (2009) Nanofibrous γ-Al_2O_3 as support for Co-based Fischer–Tropsch catalysts: pondering the relevance of diffusional and dispersion effects on catalytic performance. J Catal 263:292–305

15. Zola AS, Bidart AMF, Fraga AC, Hori CE, Sousa-Aguiar EF, Arroyo PA (2007) Cobalt supported on different zeolites for Fischer–Tropsch synthesis. Stud Surf Sci Catal 167:129–134
16. Szegedi A, Kónya Z, Méhn D, Solymar E, Pál-Borbély G, Horváth ZE, Biró AP, Kiricsi I (2004) Spherical mesoporous MCM-41 materials containing transition metals: synthesis and characterization. Appl Catal A 272:257–266
17. Tang Q, Wang Y, Zhang Q, Wan H (2003) Preparation of metallic cobalt inside NaY zeolite with high catalytic activity in Fischer–Tropsch synthesis. Catal Commun 4:253–258
18. Bessell S (1995) Investigation of bifunctional zeolite supported cobalt Fischer–Tropsch catalysts. Appl Catal A 126:235–244
19. Matsumoto A, Chen H, Tsutsumi K, Grün M, Unger K (1999) Novel route in the synthesis of MCM-41 containing framework aluminum and its characterization. Microporous Mesoporous Mater 32:55–62
20. Kresge CT, Leonowicz ME, Roth WJ, Vartulli JC, Beck JS (1992) Ordered mesoporous molecular sieves synthesized by a liquid-crystal template mechanism. Nature 359:710–712
21. Gregg SJ, Sing KSW (1982) Adsorption, surface area and porosity. Academic Press, London
22. Sing KSW, Everett DH, Haul RAW, Moscou L, Pierotti RA, Rouquérol J, Siemieniewska T (1985) Reporting physisorption data for gas/solid systems. Pure Appl Chem 57:603–619
23. Diaz JF, Balkus KJ, Bedioui F, Kurshev V, Kevan L (1997) Synthesis and characterization of cobalt-complex functionalized MCM-41. Chem Mater 9:61–67
24. Rodrigues EL, Bueno JMC (2002) Co/SiO 2 catalysts for selective hydrogenation of crotonaldehyde II: influence of the Co surface structure on selectivity. Appl Catal A 232:147–158
25. Backman LB, Rautiainen A, Lindblad M, Krause AOI (2000) Effect of support and calcination on the properties of cobalt catalysts prepared by gas phase deposition. Appl Catal A 191:55–68
26. Prieto G, Martínez A, Concepción P, Moreno-Tost R (2009) Cobalt particle size effects in Fischer–Tropsch synthesis: structural and in situ spectroscopic characterisation on reverse micelle-synthesised Co/ITQ-2 model catalysts. J Catal 266:129–144
27. Su YK, Shen CM, Yang TZ, Yang HT, Gao HJ, Li HL (2005) The dependence of Co nanoparticle sizes on the ratio of surfactants and the influence of different crystal sizes on magnetic properties. Appl Phys A 81:569–572
28. Lim S, Ciuparu D, Pak C, Dobek F, Chen Y, Harding D, Pfefferle L, Haller G (2003) Synthesis and characterization of highly ordered Co-MCM-41 for production of aligned single walled carbon nanotubes (SWNT). J Phys Chem B 107:11048–11056
29. Girardon J-S, Quinet E, Griboval-Constant A, Chernavskii PA, Gengembre L, Khodakov AY (2007) Cobalt dispersion, reducibility, and surface sites in promoted silica-supported Fischer–Tropsch catalysts. J Catal 248:143–157
30. Katsoulidis AP, Petrakis DE, Armatas GS, Trikalitis PN, Pomonis PJ (2006) Ordered mesoporous CoO x/MCM-41 materials exhibiting long-range self-organized nanostructured morphology. Microporous Mesoporous Mater 92:71–80
31. Szegedi A, Popova M, Minchev C (2009) Catalytic activity of Co/MCM-41 and Co/SBA-15 materials in toluene oxidation. J Mater Sci 44:6710–6716
32. Lou Z, Wang R, Sun H, Chen Y, Yang Y (2008) Direct synthesis of highly ordered Co-SBA-15 mesoporous materials by the pH-adjusting approach. Microporous Mesoporous Mater 110:347–354
33. Jia L, Jia L, Li D, Hou B, Wang J, Sun Y (2011) Silylated Co/SBA-15 catalysts for Fischer–Tropsch synthesis. J Solid State Chem 184:488–493
34. Tang HQ, Liew KY, Li JL (2012) Cobalt catalysts supported on silica nanotubes for Fischer-Tropsch synthesis. Sci China Chem 55:145–150
35. Friedel RA, Anderson RB (1950) Composition of synthetic liquid fuels. I. product distribution and analysis of C5—C8 paraffin isomers from cobalt catalyst1. J Am Chem Soc 72:1212–1215